

Synergistically boosting the elementary reactions over multiheterogeneous ordered macroporous Mo₂C/NC-Ru for highly efficient alkaline hydrogen evolution

Kaixi Wang¹ | Shuo Wang¹ | Kwan San Hui² | Haixing Gao¹ |
 Duc Anh Dinh³ | Chengzong Yuan¹ | Chenyang Zha¹  | Zongping Shao^{4,5}  |
 Zikang Tang¹ | Kwun Nam Hui¹ 

¹Joint Key Laboratory of the Ministry of Education, Institute of Applied Physics and Materials Engineering, University of Macau, Taipa, Macau SAR, China

²School of Engineering, Faculty of Science, University of East Anglia, Norwich, UK

³NTT Hi-Tech Institute, Nguyen Tat Thanh University, Ho Chi Minh City, Vietnam

⁴State Key Laboratory of Materials-Oriented Chemical Engineering, College of Chemical Engineering, Nanjing Tech University, Nanjing, China

⁵WA School of Mines: Minerals, Energy and Chemical Engineering (WASM-MECE), Curtin University, Perth, Western Australia, Australia

Correspondence

Kwan San Hui, School of Engineering,
 Faculty of Science, University of East
 Anglia, Norwich, NR4 7TJ, UK.
 Email: k.hui@uea.ac.uk

Zongping Shao, State Key Laboratory of
 Materials-Oriented Chemical Engineering,
 College of Chemical Engineering, Nanjing
 Tech University, 211816 Nanjing, China.
 Email: shaozp@njtech.edu.cn

Kwun Nam Hui, Joint Key Laboratory of
 the Ministry of Education, Institute of
 Applied Physics and Materials
 Engineering, University of Macau,
 Avenida da Universidade, Taipa, Macau
 SAR 999078, China.
 Email: bizhui@um.edu.mo

Funding information

University of Macau,
 Grant/Award Numbers: MYRG2018-
 00192-IAPME, MYRG2020-00187-IAPME;
 Science and Technology Development
 Fund, Macau SAR,
 Grant/Award Numbers: 0021/2019/AIR,
 0041/2019/A1, 0046/2019/AFJ, 0191/2017/
 A3; UEA funding

Abstract

Simultaneously enhancing the reaction kinetics, mass transport, and gas release during alkaline hydrogen evolution reaction (HER) is critical to minimizing the reaction polarization resistance, but remains a big challenge. Through rational design of a hierarchical multiheterogeneous three-dimensionally (3D) ordered macroporous Mo₂C-embedded nitrogen-doped carbon with ultrafine Ru nanoclusters anchored on its surface (OMS Mo₂C/NC-Ru), we realize both electronic and morphologic engineering of the catalyst to maximize the electrocatalysis performance. The formed Ru-NC heterostructure shows regulative electronic states and optimized adsorption energy with the intermediate H*, and the Mo₂C-NC heterostructure accelerates the Volmer reaction due to the strong water dissociation ability as confirmed by theoretical calculations. Consequently, superior HER activity in alkaline solution with an extremely low overpotential of 15.5 mV at 10 mA cm⁻² with the mass activity more than 17 times higher than that of the benchmark Pt/C, an ultrasmall Tafel slope of 22.7 mV dec⁻¹, and excellent electrocatalytic durability were achieved, attributing to the enhanced mass transport and favorable gas release process endowed from the unique OMS Mo₂C/NC-Ru structure. By oxidizing OMS Mo₂C/NC-Ru into OMS MoO₃-RuO₂ catalyst, it can also be applied as efficient oxygen evolution electrocatalyst, enabling the

Kaixi Wang and Shuo Wang contributed equally to this study.

This is an open access article under the terms of the Creative Commons Attribution License, which permits use, distribution and reproduction in any medium, provided the original work is properly cited.

© 2022 The Authors. *Carbon Energy* published by Wenzhou University and John Wiley & Sons Australia, Ltd.

construction of a quasi-symmetric electrolyzer for overall water splitting. Such a device's performance surpassed the state-of-the-art Pt/C || RuO₂ electrolyzer. This study provides instructive guidance for designing 3D-ordered macroporous multicomponent catalysts for efficient catalytic applications.

KEYWORDS

heterostructure, hydrogen evolution reaction, molybdenum carbide, ordered macroporous structure, ruthenium nanoparticle, synergistic effect

1 | INTRODUCTION

Climate change due to the excessive use of fossil fuels has been pushing people to explore new carbon-neutral renewable energy sources.^{1,2} Hydrogen, as one of the most promising alternatives, has attracted great attention owing to its high energy density, sustainability, and cleanliness.^{3–5} Water electrolysis using renewable energy input (such as solar and wind energy) provides an attractive and eco-friendly approach for large-scale hydrogen production.^{6–8} Compared with the acidic water splitting technique, the alkaline water splitting in anion-exchange-membrane water electrolyzers (AEMWEs) can reduce the damage of electrolyte to metal-based electrode materials and increase the choices of available electrocatalysts due to the milder alkaline working environment.⁹ Therefore, the research on AEMWEs has become a hot topic in the field of energy conversion. Till now, even in alkaline solution, platinum (Pt)-based materials are still the benchmark electrocatalysts for electrochemical hydrogen evolution reaction (HER) due to their high activity. However, the Earth's scarcity and high price severely hinder their widespread application.^{10,11} To reduce the cost, it is highly imperative to design Pt-free HER catalysts with Pt-comparable activity in an alkaline medium.

As a much cheaper noble metal in the Pt group (only one-third the price of Pt), ruthenium (Ru) exhibits a similar bond strength with hydrogen (ca. 65 kcal mol⁻¹) to that of Pt and a favorable chemical inertness to corrosive electrolyte, making it a promising substitute to Pt.^{12–14} Although Ru possesses potentially high electrocatalytic activity for HER, the active Ru nanoparticles (NPs) tend to agglomerate because of the large cohesive energy, resulting in decreased activity.^{15,16} To resolve this issue, some conductive substrates, especially carbon materials (carbon nanotube,¹⁶ graphene,^{17,18} carbon nanofiber,¹⁹ carbon dot,^{20,21} C₂N,²² various precursor-derived carbon,^{23–25} etc.) were often utilized to anchor Ru NPs due to their high conductivity, good stability, and rich functional groups. The carbon support not only provides fast electron transfer but also forms a

heterostructure with Ru NPs, which could regulate the local electronic structures and hydrogen adsorption free energy (ΔG_{H^*}) of the active sites due to the strong metal-support interaction, thereby modifying the electrocatalytic activity and stability.^{18,22,23} However, ΔG_{H^*} alone is hardly sufficient to describe the activity of HER in alkaline solutions²⁶ because of its multistep process in nature. Actually, the Volmer step ($H_2O + * + e^- \rightarrow H^* + OH^-$) and the Heyrovsky step ($H^* + H_2O + e^- \rightarrow H_2 + * + OH^-$) or the Tafel step ($H^* + H^+ + e^- \rightarrow H_2 + *$) act together to affect the overall HER activity.^{27,28} In this case, considering the relatively high-energy barrier for water dissociation of Ru,²⁶ a well-designed substrate with good water dissociation ability is essential to achieving efficient electrocatalysis for alkaline HER. Previous work has confirmed that Mo₂C possesses a low water dissociation energy in alkali,^{29,30} and thus a carbon–Mo₂C composite support may be a good choice for Ru anchoring.

In addition, to improve the intrinsic activity of electrocatalysts, additional attention should be paid to the mass transport of reactants and hydrogen products during the HER process. While the porous structure could facilitate the mass transfer of reactants, the generated large amount of gas bubbles in the pores might hinder the approach of reactants and shield the catalytically active sites, especially at high current densities, leading to a limited hydrogen production rate.^{31,32} Moreover, the bubbles are easily blocked and trapped as they transport through the disordered porous structure, which is not favorable for their rapid release.^{33,34} Compared to a commonly disordered porous structure containing micropores and mesopores, the well-defined hierarchically porous structure with three-dimensionally (3D) ordered macropores not only guarantees fast mass transfer of reactants but also helps to realize a high gas release rate.^{35,36} Taking into account the above views, it is believed that coupling Ru NPs with appropriate carbon–Mo₂C composite support that possesses hierarchically ordered macroporous structure may achieve superior overall HER performance in alkaline, but this kind of electrocatalyst is rarely explored.

Herein, we reported the rational design of a hierarchically multiheterogeneous OMS Mo₂C/NC-Ru

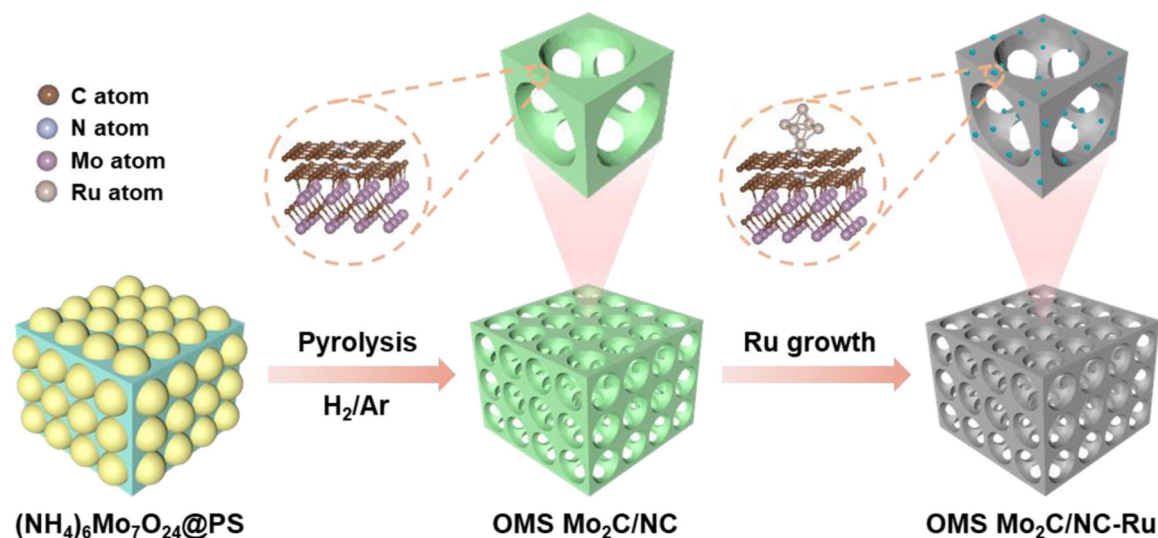
composite by selecting a 3D-ordered macroporous Mo₂C-embedded nitrogen-doped carbon (OMS Mo₂C/NC) as support to couple with Ru nanoclusters. The unique structure of OMS Mo₂C/NC-Ru brought about superior HER performance in 1.0 M KOH electrolyte with an extremely low overpotential of 15.5 mV at a current density of 10 mA cm⁻², an ultrasmall Tafel slope of 22.7 mV dec⁻¹, and more than 17 times higher mass activity compared to the benchmark Pt/C electrocatalyst. In addition, after a 100-h long-term cyclic test from 10 to 100 mA cm⁻² using the multicurrent chronopotentiometric method, the overpotential was not changed. Density functional theory (DFT) calculations manifest that the formed Ru-NC heterostructure displayed regulative electronic states and optimized adsorption energy with the intermediate H*; at the same time, the Mo₂C-NC heterostructure accelerates the Volmer reaction to offer a much faster proton supply due to the strong water dissociation ability. Thus, the multiheterogeneous synergy greatly boosts the overall HER kinetics in alkaline conditions. After assembling with OMS Mo₂C/NC-Ru-derived ordered macroporous MoO₃-RuO₂ superstructure (OMS MoO₃-RuO₂) electrode, the quasi-symmetric electrolyzer requires only a low voltage of 1.62 V to reach 10 mA cm⁻², much better than that of the state-of-the-art Pt/C || RuO₂ pair.

2 | RESULTS AND DISCUSSION

The synthesis process of the OMS Mo₂C/NC-Ru composite is schematically shown in Scheme 1, which consists of two main steps. First, monodisperse polystyrene spheres

(PSs; ~270 nm) were assembled into a 3D-ordered PS template through vacuum filtration (Figure S1), and then an ammonium molybdate tetrahydrate solution was filled into the PS template voids to obtain the (NH₄)₆Mo₇O₂₄@PS precursor (Figure S2), followed by pyrolysis of the precursor at 750°C under H₂/Ar atmosphere to decompose PS with the formation of the OMS Mo₂C/NC. The OMS Mo₂C/NC-Ru catalyst was then prepared by reducing Ru³⁺ with sodium borohydride (NaBH₄) in the presence of OMS Mo₂C/NC as the support, followed by subsequent thermal treatment under inert atmospheres.

The scanning electron microscopy (SEM) and transmission electron microscopy (TEM) images of the as-prepared OMS Mo₂C/NC substrate (Figure S3A–C) unveils a 3D framework structure with ordered macroporous cavities (~260 nm) interconnected by macroporous channels with a size of about 110 nm. Figure S3D,E shows that the Mo₂C nanoparticles were embedded in an NC skeleton with several layers of NC on the surface. The high-angle annular darkfield scanning transmission electron microscopy (HAADF-STEM) image and corresponding elemental mappings of OMS Mo₂C/NC (Figure S3F) reveals a homogeneous distribution of C, N, and Mo elements in the 3D-ordered macroporous architecture. The X-ray diffraction (XRD) pattern and X-ray photoelectron spectroscopy (XPS) spectrum (Figure S4) further demonstrates the successful formation of the ordered OMS Mo₂C/NC structure with good crystallinity. In addition, we found that the reduced gas environment and PS template were essential for the formation of OMS Mo₂C/NC with a pure Mo₂C phase. Under the N₂ atmosphere, only a mixed phase of molybdenum carbide, oxide, and nitride was obtained (Figure S5). Moreover, in this study, PS was used not only



SCHEME 1 Schematic illustration of the synthetic process of ordered macroporous Mo₂C-embedded nitrogen-doped carbon with ultrafine Ru nanoclusters anchored on its surface (OMS Mo₂C/NC-Ru). PS, polystyrene sphere

as a template but also as a carbon source, despite its complete degradation and volatilization in an inert gas (Figure S6), which may be due to the fact that the generated Mo metal transition phase catalyzed the small molecular hydrocarbons produced by PS decomposition during the pyrolysis (Figure S7), thereby forming a carbon layer deposited on the surface of Mo_2C .

The multiheterogeneous OMS $\text{Mo}_2\text{C}/\text{NC-Ru}$ was obtained by simply coupling Ru NPs with the OMS $\text{Mo}_2\text{C}/\text{NC}$ support. The crystal structure of OMS $\text{Mo}_2\text{C}/\text{NC-Ru}$ was analyzed by XRD (Figure 1A). All the diffraction peaks can be well indexed based on the hexagonal $\beta\text{-Mo}_2\text{C}$ (PDF#35-0787),³⁷ whereas no obvious characteristic peaks of Ru NPs were observed, indicating the low content and ultrasmall size of the Ru NPs.²³ The morphology of the catalyst was characterized by SEM and TEM. The SEM images of OMS $\text{Mo}_2\text{C}/\text{NC-Ru}$ (Figures 1B and S8A,B) demonstrate that the

ordered macroporous structure was well preserved without significant change in the dimension of macropores after the implantation of Ru. The TEM image also confirms the ordered macroporous framework of OMS $\text{Mo}_2\text{C}/\text{NC-Ru}$ (Figure 1C). Besides, some mesopores were observed on the wall of the macropore (Figure 1D), demonstrating the hierarchically porous structure of the sample, which can effectively enhance the accessibility of the active sites to reactants.^{38,39} A magnified TEM image (Figure 1E) clearly discloses a homogeneous distribution of the ultrafine Ru nanoclusters (average diameter $\sim 2.5 \pm 0.5$ nm) on the ordered macroporous framework. The loading of Ru nanoclusters in the OMS $\text{Mo}_2\text{C}/\text{NC-Ru}$ sample was estimated to be 1.75 wt% by the inductively coupled plasma–optical emission spectrometer (ICP-OES). The high-resolution TEM (HRTEM) image (Figure 1F) further reveals the co-existence of Ru and Mo_2C phases. The lattice fringes with

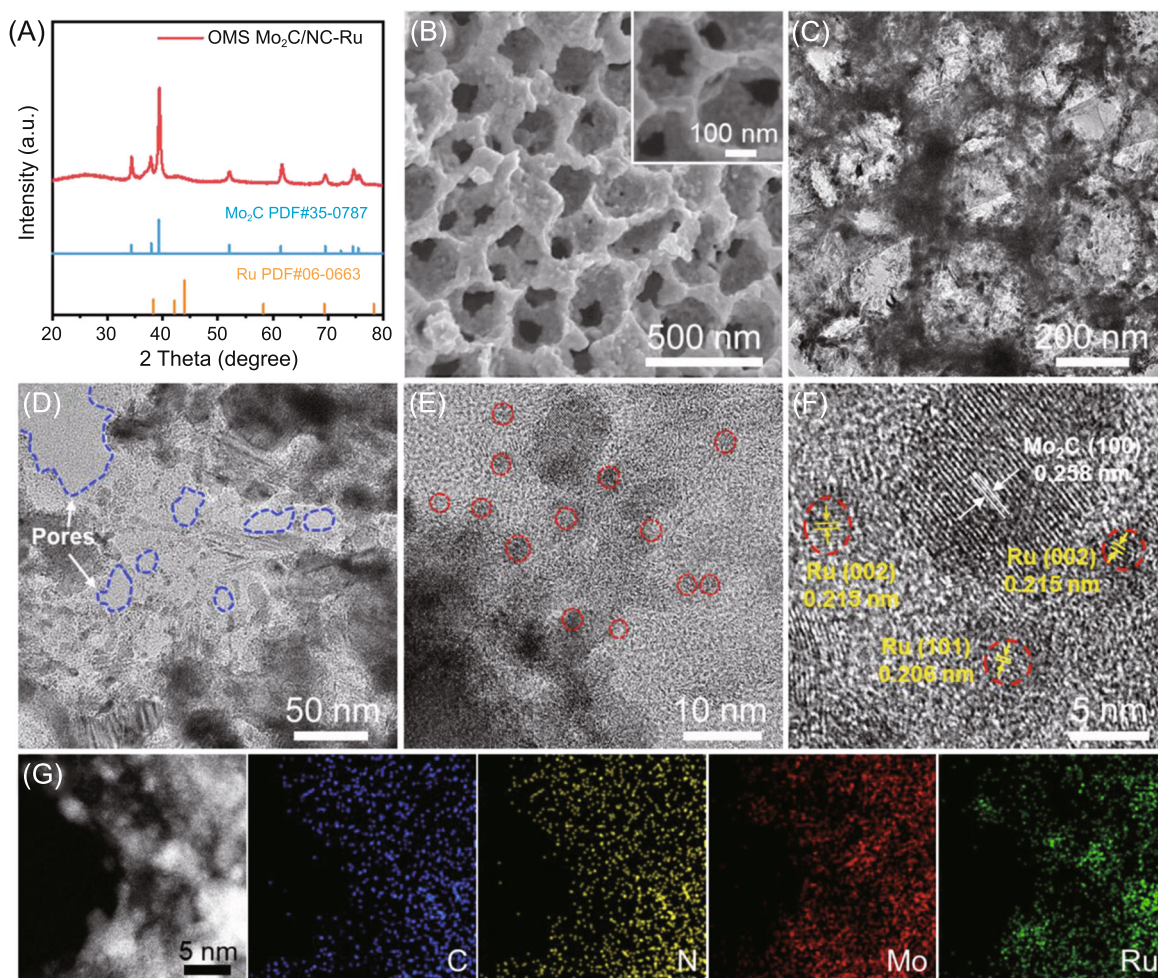


FIGURE 1 (A) X-ray diffraction pattern, (B) SEM image (inset shows a magnified SEM image), and (C–E) transmission electron microscopy (TEM) images of ordered macroporous Mo_2C -embedded nitrogen-doped carbon with ultrafine Ru nanoclusters anchored on its surface (OMS $\text{Mo}_2\text{C}/\text{NC-Ru}$). (F) High-resolution TEM image of OMS $\text{Mo}_2\text{C}/\text{NC-Ru}$. (G) High-angle annular darkfield scanning transmission electron microscopy image and the corresponding energy-dispersive X-ray spectroscopy elemental mappings of OMS $\text{Mo}_2\text{C}/\text{NC-Ru}$ for C, N, Mo, and Ru elements

spacings of 0.206 and 0.215 nm can be indexed to the (101) and (002) planes of hexagonal Ru, respectively, and the lattice fringes with a spacing of 0.258 nm are attributed to Mo₂C. Moreover, the HAADF-STEM images and corresponding element mappings (Figures 1G and S8C,D) further proved the successful formation of uniform ultrafine Ru nanoclusters anchoring on the hierarchically ordered macroporous Mo₂C/NC superstructure, as evidenced by the even distribution of C, N, Mo, and Ru elements in the whole OMS Mo₂C/NC-Ru architecture. For comparison, solid Mo₂C/NC-Ru was also synthesized by the same procedure except that the precursor was replaced by the mixture of disordered PSs powder and ammonium molybdate tetrahydrate. The solid Mo₂C/NC-Ru showed a solid granular structure with homogeneous elements distribution in the architecture exempt of 3D interconnected ordered macropores (Figures S9 and S10). XRD and XPS results confirm the formation of the solid Mo₂C/NC-Ru sample (Figure S11).

The pore structure characteristics of OMS Mo₂C/NC-Ru were investigated by N₂ sorption measurements (Figure 2A). The adsorption/desorption behavior showed a combined II/IV-type isotherm with H3-type hysteresis loop, confirming

the presence of plentiful mesopores,⁴⁰ consistent with the TEM observation. OMS Mo₂C/NC-Ru possessed a larger Brunauer–Emmett–Teller (BET) surface area of 51.7 m² g⁻¹ than OMS Mo₂C/NC (38.1 m² g⁻¹) and solid Mo₂C/NC-Ru (40.0 m² g⁻¹, Figure S12), which is mainly ascribed to the incorporation of ultrafine Ru nanoclusters in the hierarchically macroporous structure. Raman spectroscopy was used to evaluate the disorder in carbon materials. Similar I_D/I_G ratio of OMS Mo₂C/NC-Ru and OMS Mo₂C/NC indicates that the coupling of Ru nanoclusters had little influence on the structure of N-doped carbon (Figure 2B). A higher I_D/I_G ratio of OMS Mo₂C/NC-Ru suggests that it possessed more defects on NC than solid Mo₂C/NC-Ru (Figure S13), which is favorable for improving the HER performance.¹²

XPS analysis was employed to get insight into the elemental and chemical state of the catalyst surface. The full XPS survey spectrum shows the presence of C, N, Mo, Ru, and O elements in the OMS Mo₂C/NC-Ru sample (Figure S14). The high-resolution C 1s spectrum can be divided into four peaks with binding energies of 284.7, 285.6, 286.5, and 288.8 eV, corresponding to C–C/C=C, C–N, C–O, and O–C=O, respectively.^{25,36}

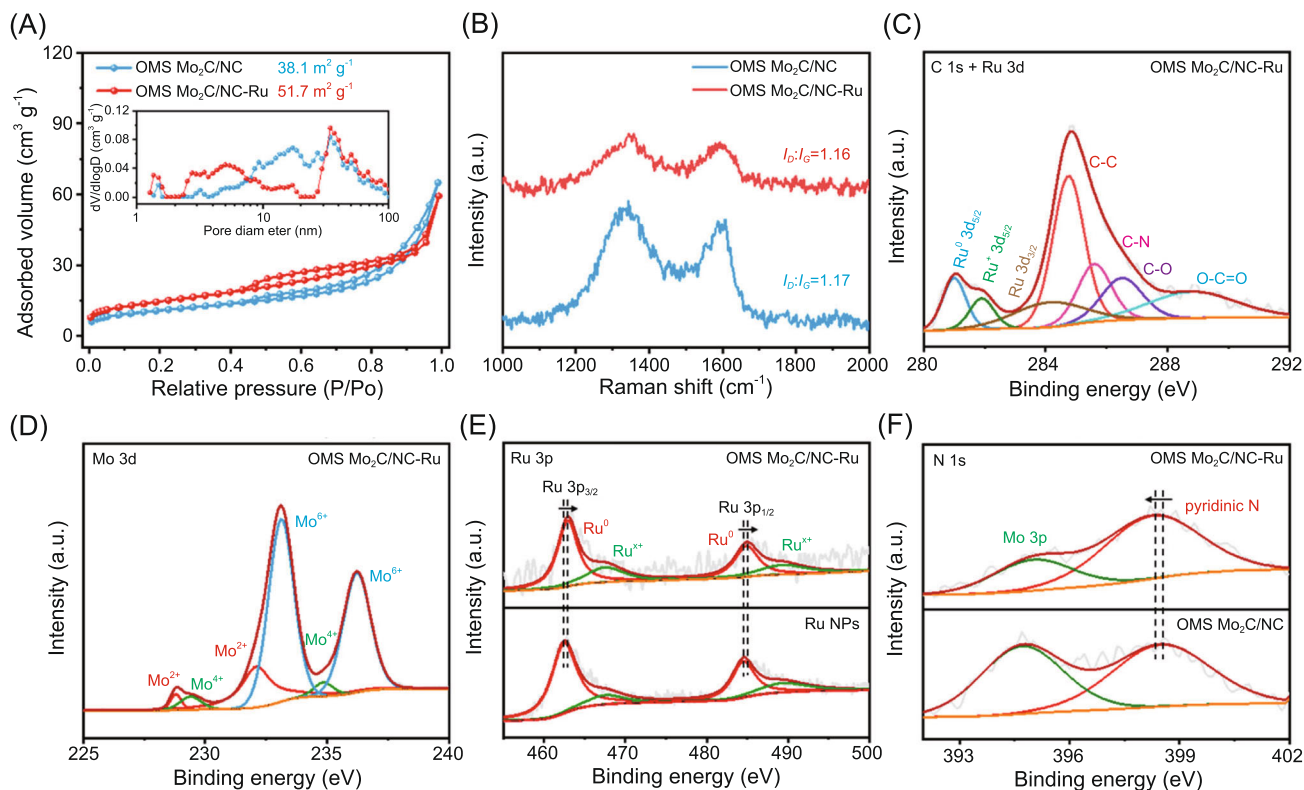


FIGURE 2 (A) N₂ sorption isotherms and (B) Raman spectra of OMS Mo₂C/NC and OMS Mo₂C/NC-Ru. Inset in (A) shows the corresponding pore size distribution. (C) High-resolution C 1s + Ru 3d and (D) Mo 3d XPS spectra of OMS Mo₂C/NC-Ru. (E) High-resolution Ru 3p XPS spectrum of OMS Mo₂C/NC-Ru and Ru NPs. (F) High-resolution N 1s XPS spectra of OMS Mo₂C/NC-Ru and OMS Mo₂C/NC. NP, nanoparticle; OMS Mo₂C/NC-Ru, ordered macroporous Mo₂C-embedded nitrogen-doped carbon with ultrafine Ru nanoclusters anchored on its surface; XPS, X-ray photoelectron spectroscopy

The partially coincident Ru 3d signal peaks, existing at 281.0 and 284.2 eV, were assigned to the Ru 3d_{5/2} and Ru 3d_{3/2} of the metal Ru, respectively, while the peak at 281.9 eV was related to the oxidized Ru species (Figure 2C).^{29,41} In the Mo 3d spectrum, the Mo⁴⁺ and Mo⁶⁺ signals were also observed except Mo²⁺, attributed to the unavoidable surface oxidation of Mo species when exposed to air (Figure 2D).^{42,43} To understand the electronic state of Ru in OMS Mo₂C/NC-Ru, pure Ru NPs were also prepared for comparison (Figure S15). From the deconvoluted spectrum of Ru 3p (Figure 2E), two peaks at 462.9 and 484.9 eV were attributed to Ru 3p_{3/2} and Ru 3p_{1/2} of metallic Ru,^{12,21} respectively, while the other two peaks were associated with surface-oxidized Ru species caused by the exposure to air. Besides, the Ru 3p peak of OMS Mo₂C/NC-Ru showed a positive shift of 0.4 eV compared with that of Ru NPs, suggesting the increased valence state of Ru in OMS Mo₂C/NC-Ru due to the strong interaction between Ru metal and the Mo₂C/NC support. At the same time, the N 1s peak of OMS Mo₂C/NC-Ru displayed a negative shift compared with that of OMS Mo₂C/NC (Figure 2F), which certified the electron transfer from Ru to N.

The electrocatalytic performance toward HER of OMS Mo₂C/NC-Ru was investigated in an alkaline solution (1.0 M KOH) using a standard three-electrode system. Pure Ru NPs, OMS Mo₂C/NC, solid Mo₂C/NC-Ru, and commercial 20% Pt/C were also measured for comparison. Figure 3A shows the *i*R-corrected HER linear sweep voltammetry (LSV) curves of different catalysts. Pure Ru NPs and OMS Mo₂C/NC achieved a current density of 10 mA cm⁻² at a relatively high overpotential of 61.9 and 124.1 mV, respectively, while when coupling them together to form a multiheterogeneous OMS Mo₂C/NC-Ru structure, the overpotential was sharply decreased to 15.5 mV, demonstrating the synergistic effect between Ru NPs and Mo₂C/NC toward HER catalysis. Notably, OMS Mo₂C/NC-Ru showed lower overpotential than solid Mo₂C/NC-Ru (39.3 mV) and Pt/C (23.3 mV). Besides, OMS Mo₂C/NC-Ru displayed the lowest overpotential of 42.7 mV at 50 mA cm⁻², surpassing all control catalysts (Figure 3B). The Tafel slopes derived from LSV curves were employed to evaluate the HER kinetics. Figure 3C shows that the Tafel slope for OMS Mo₂C/NC-Ru is 22.7 mV dec⁻¹, smaller than that of Pt/C (28.1 mV dec⁻¹) and other samples, signifying more efficient hydrogen evolution kinetics and dominant Volmer-Tafel mechanism in the HER pathway.^{12,44} From the Tafel plots, the exchange current density of OMS Mo₂C/NC-Ru is 2.08 mA cm⁻² (Figure S16), which is much larger than those of other catalysts and even higher than that of Pt/C (1.64 mA cm⁻²), indicating its intrinsic rapid HER kinetics.^{16,45}

Impressively, the comparison of activity with other recently reported high-performance HER electrocatalysts demonstrates that our catalyst ranks among the top alkaline HER electrocatalysts (Figure 3D and Table S1). We further evaluated the mass activities of noble metals (Ru and Pt) in OMS Mo₂C/NC-Ru and Pt/C by normalizing the LSV curves. As shown in Figure 3E, OMS Mo₂C/NC-Ru possessed extraordinarily high mass activity compared to Pt/C in which, at an overpotential of 50 mV, OMS Mo₂C/NC-Ru showed the mass activity of 1.118 A mg⁻¹_{Ru}, 17.8 times higher than that of Pt/C (0.0627 A mg⁻¹_{Pt}). The high mass activity of the catalyst is undoubtedly conducive to its low-cost practical applications.

As an important parameter, the electrochemical surface area (ECSA) for HER was estimated by the electrochemical double-layer capacitance (*C*_{dl}) in a non-Faradaic region (Figure S17). As shown in Figure 3F, OMS Mo₂C/NC-Ru exhibited the *C*_{dl} of 15.5 mF cm⁻², which is higher than those of OMS Mo₂C/NC (3.5 mF cm⁻²), Ru NPs (4.8 mF cm⁻²), and Solid Mo₂C/NC-Ru (9.9 mF cm⁻²), indicating that coupling Ru nanoclusters with the hierarchically ordered macroporous Mo₂C/NC is beneficial to exposing more active sites, thus enhancing the catalytic activities.³⁶ Electrochemical impedance spectroscopy was further performed to study the interfacial electron transfer dynamics during the HER process. OMS Mo₂C/NC-Ru demonstrated the smallest charge transfer resistance (*R*_{ct}) of 1.75 Ω (Figures 3G and S18), suggesting the fastest charge transfer at the interface of OMS Mo₂C/NC-Ru and the electrolyte, which improved the HER performance. The dynamic water contact angle measurement confirmed the superior hydrophilic nature of OMS Mo₂C/NC-Ru (Figure S19), indicating that the hierarchically ordered macroporous architecture facilitated the penetration of the electrolyte and enhanced the mass transport.^{25,46-48} Notably, such a unique OMS Mo₂C/NC-Ru structure endowed the superior hydrophilicity, which is favorable for activating water molecules and accelerating the Volmer step in the HER process.²⁸ To get more insights into the active sites of OMS Mo₂C/NC-Ru, thiocyanate ions (SCN⁻) were added to the KOH electrolyte as metal-centered active site poisoners (Figure S20). It was found that the current density of OMS Mo₂C/NC-Ru decreased dramatically with the loss ratio of 85.1% upon the addition of SCN⁻, indicating that the active sites were blocked by SCN⁻. As a comparison, the current density of OMS Mo₂C/NC decreased relatively slowly, with the loss ratio of 28.4%, which unveils Ru nanoclusters as the major active sites of the OMS Mo₂C/NC-Ru catalyst.

The electrocatalytic durability of OMS Mo₂C/NC-Ru was examined to evaluate the HER performance.

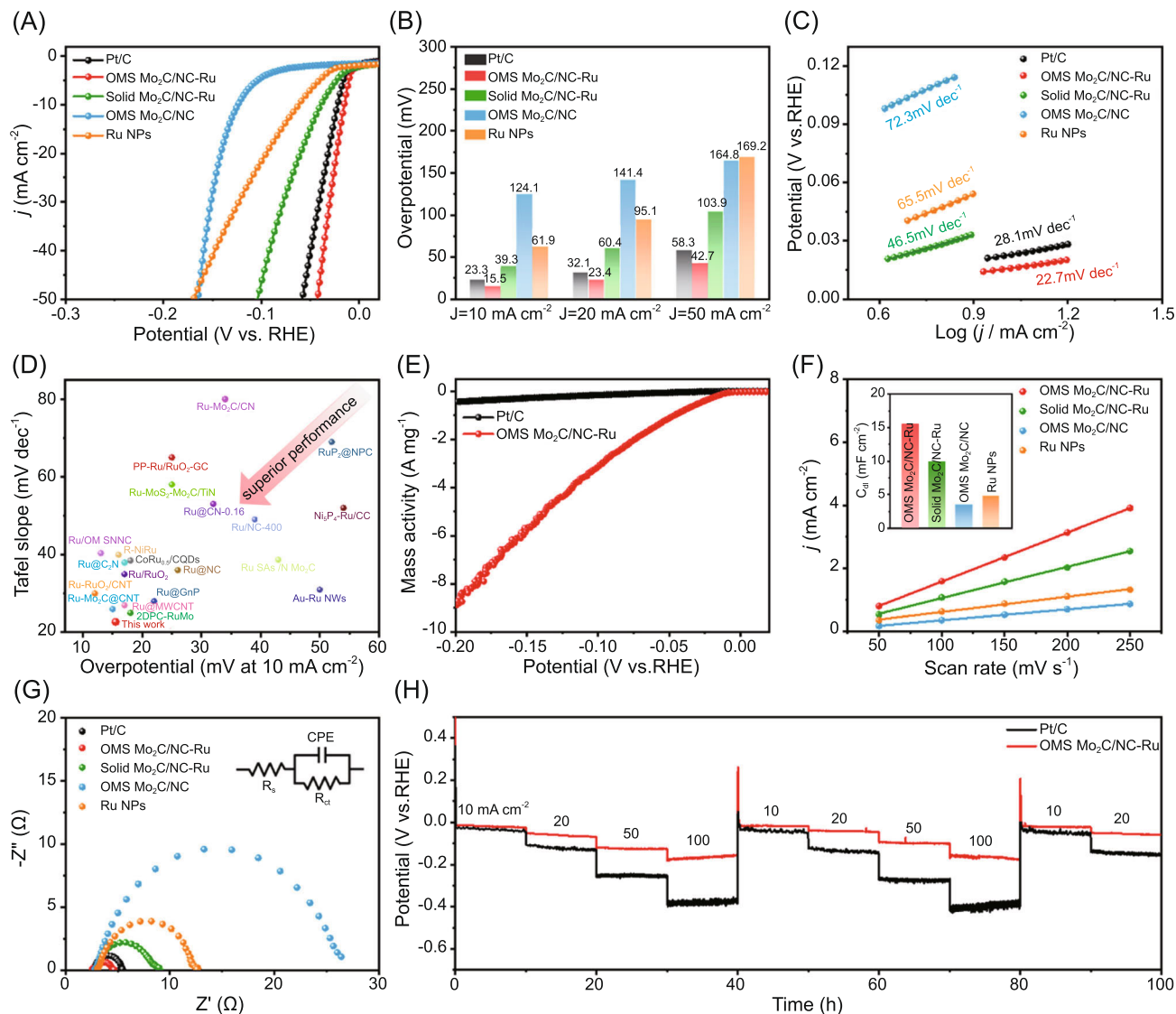


FIGURE 3 Electrocatalytic HER performance evaluation of various catalysts in 1.0 M KOH. (A) HER polarization curves of Pt/C, OMS Mo₂C/NC-Ru, solid Mo₂C/NC-Ru, OMS Mo₂C/NC, and Ru NPs catalysts with iR correction. (B) Comparison of overpotential changes at 10, 20, and 50 mA cm⁻². (C) Tafel plots obtained from the polarization curves in (A). (D) Comparison of the Tafel slope and overpotential at 10 mA cm⁻² in 1.0 M KOH for OMS Mo₂C/NC-Ru with other recently reported HER catalysts. (E) Mass activities of OMS Mo₂C/NC-Ru and Pt/C. (F) The differences in current density (Δj) at 0.975 V (vs. RHE) as a function of scan rate for OMS Mo₂C/NC-Ru, solid Mo₂C/NC-Ru, OMS Mo₂C/NC, and Ru NPs. Inset is the corresponding C_{dl} values. (G) Electrochemical impedance spectroscopy of Pt/C, OMS Mo₂C/NC-Ru, solid Mo₂C/NC-Ru, OMS Mo₂C/NC, and Ru NPs. Inset is the equivalent circuit in which R_s , R_{ct} , and CPE are solution resistance, charge transfer resistance between catalyst and electrolyte, and constant phase element, respectively. (H) Multicurrent chronopotentiometric curves of OMS Mo₂C/NC-Ru and Pt/C with iR correction. HER, hydrogen evolution reaction; NP, nanoparticle; OMS Mo₂C/NC-Ru, ordered macroporous Mo₂C-embedded nitrogen-doped carbon with ultrafine Ru nanoclusters anchored on its surface

The LSV curves almost remained unchanged and the overpotential showed an inappreciable decline before and after 5000 cyclic voltammetry (CV) cycles (Figure S21), demonstrating good long-term stability, which was also verified by the $i-t$ chronoamperometric response of OMS Mo₂C/NC-Ru over 40 h. Additionally, the multicurrent chronopotentiometric measurement was carried out to further assess the outstanding stability of OMS Mo₂C/NC-Ru with Pt/C as a contrast

(Figure 3H). It can be seen that OMS Mo₂C/NC-Ru exhibited better stability throughout the 100 h cyclic test at different current densities from 10 to 100 mA cm⁻² with smaller overpotential increments as the current density increases. Significantly, the curve of Pt/C is rougher than that of OMS Mo₂C/NC-Ru, especially at high current densities of 100 mA cm⁻², suggesting a greater disturbance to the Pt/C catalyst by plenty of gas bubbles in the HER process, which may be ascribed to the lack of

hierarchically ordered macropores for fast gas release. Meanwhile, we studied the change of the structure and composition of OMS Mo₂C/NC-Ru before and after HER. The ordered macroporous structure was well maintained after the stability test (Figures S22 and S23) and the composition was basically unchanged (Figure S24). These results indicate the superior chemical and structural stability of OMS Mo₂C/NC-Ru catalyst during the HER process, which are the cornerstone of the excellent electrocatalytic performance.

To elucidate the underlying mechanism of superior HER activity of OMS Mo₂C/NC-Ru, DFT calculations were conducted. The theoretical models of Ru, Ru-NC,

and Mo₂C-NC heterointerfaces were established based on the experimental observation and analysis (Figures 4A and S25). In alkaline media, favorable H₂O adsorption on catalysts is important for subsequent effective H₂O activation.⁴⁹ Compared with Ru-NC, Mo₂C-NC has a lower H₂O adsorption energy value of -0.64 eV (Figure 4B), leading to much faster H₂O adsorption on the surface of Mo₂C-NC, which is beneficial to activating water molecules and accelerating the first step of Volmer reaction.^{22,28} In addition, the rapid dissociation of adsorbed H₂O into H* and *OH guarantees sufficient protons for the overall reaction. As shown in Figure 4C, the dissociation of H₂O on the surface of Mo₂C-NC is much easier

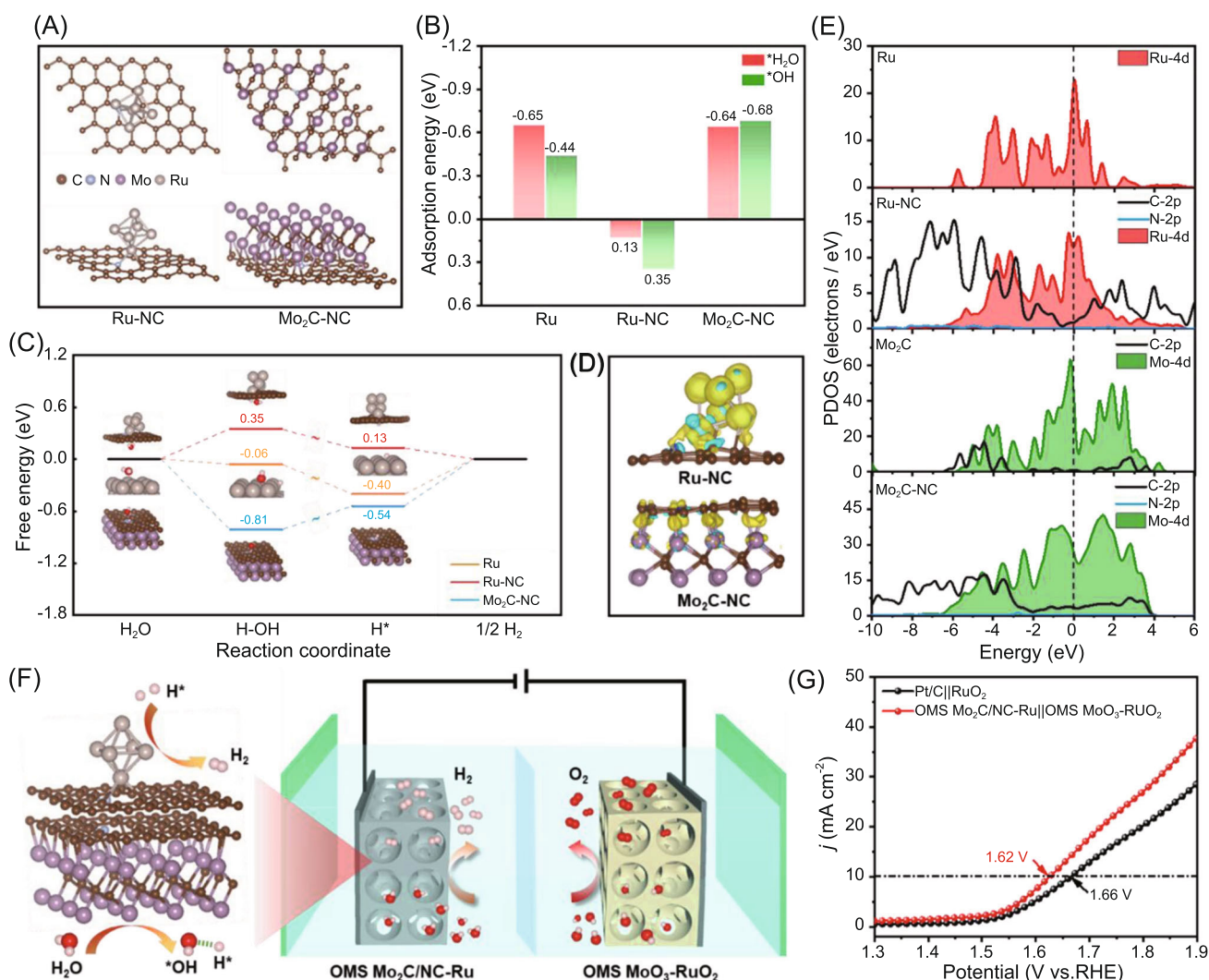


FIGURE 4 (A) Structures of Ru-NC and Mo₂C-NC. (B) Adsorption energies of H₂O and OH⁻ on Ru, Ru-NC, and Mo₂C-NC. (C) Gibbs free energy diagram for HER on Ru, Ru-NC, and Mo₂C-NC. Insets are the geometric configurations of the *H₂O, H* + *OH, and H* adsorbed on Ru, Ru-NC, and Mo₂C-NC. (D) Side view of charge density differences in the heterostructures for Ru-NC and Mo₂C-NC. (E) Density of states (DOS) of Ru, Ru-NC, Mo₂C, and Mo₂C-NC systems. (F) Schematic representation for the overall alkaline water splitting. (G) Polarization curves of the OMS Mo₂C/NC-Ru || OMS MoO₃-RuO₂ and Pt/C || RuO₂ pairs for water splitting. HER, hydrogen evolution reaction; OMS Mo₂C/NC-Ru, ordered macroporous Mo₂C-embedded nitrogen-doped carbon with ultrafine Ru nanoclusters anchored on its surface

compared with those on the surfaces of Ru-NC and Ru, indicating the faster proton supply by the Mo₂C-NC carrier. As more *OH adsorbed on the surface of catalysts may decrease the HER efficiency, we further calculated and compared the adsorption energy of *OH (Figure 4B). Results show that the formation of Ru-NC heterojunction results in weaker attraction to *OH compared with pure Ru. Besides, *OH tends to be adsorbed on the surface of Mo₂C-NC due to the lower adsorption energy, suggesting that *OH adsorption on Ru-NC may transfer to that on Mo₂C-NC, and more active sites in Ru-NC can be released for H* adsorption, thus promoting the Tafel step. Moreover, ΔG_{H^*} is widely used as a critical activity descriptor to evaluate HER performance, and a ΔG_{H^*} value close to 0 eV is satisfactory.^{50,51} The calculated ΔG_{H^*} values of Ru and Mo₂C-NC are -0.4 and -0.54 eV, respectively, which indicates their strong hydrogen adsorption and unfavorable release process. In contrast, the ΔG_{H^*} value at the Ru-NC heterointerface is 0.13 eV, closer to 0, proving its faster hydrogen absorption/desorption kinetics.

To further gain perceptions about the activity origin of OMS Mo₂C/NC-Ru, the intrinsic electronic states of the formed Ru-NC and Mo₂C-NC heterointerfaces were calculated. The charge density difference plots reveal that the charge density is redistributed at the constructed heterointerface (Figures 4D and S26) and the electrons transfer from Ru atoms to N atoms, which is consistent with the XPS analysis. The modulated electronic structure is conducive for appropriate adsorption/desorption behavior of reaction intermediates, thus enhancing the catalytic activity. Additionally, in the heterostructures, the density of states (DOS) occupied by the metal d-orbital at the Fermi level is significantly weakened and the overall DOS is more diffuse (Figure 4E), leading to weaker adsorption of the reactants, which is also consistent with the above DFT results. In brief, these theoretical results demonstrate that the Mo₂C-NC heterojunctions accelerate the water adsorption and dissociation in the Volmer step, and the Ru-NC heterojunctions exhibit an optimized H* adsorption/desorption behavior in the Tafel step (Figure 4F), therefore resulting in outstanding HER performance of multi-heterogeneous OMS Mo₂C/NC-Ru in alkaline solution.

Considering the impressive HER performance of OMS Mo₂C/NC-Ru, it is encouraged to achieve practical overall water splitting by coupling a suitable oxygen evolution reaction (OER) catalyst. Inspired by the good OER activity of commercial RuO₂, a series of RuO₂-based catalysts were prepared by annealing OMS Mo₂C/NC-Ru in the air at different temperatures. The derived materials were denoted as OMS MoO₃-RuO₂-X (X represents the temperature) according to the XRD patterns (Figure S27). The OER activities of the as-synthesized OMS MoO₃-RuO₂-X were measured using a typical three-electrode system under

1.0 M KOH and compared with that of commercial RuO₂. Figure S28 displays that the OMS MoO₃-RuO₂ (derived at 450°C) only needs an overpotential of 380 mV to reach 10 mA cm⁻², which is 38 mV lower than that of RuO₂ catalyst. The morphology and structure analysis confirmed the formation of OMS MoO₃-RuO₂ with small RuO₂ NPs loaded on the surface of MoO₃ (Figures S29–S31). Then, we assembled a two-electrode cell using OMS Mo₂C/NC-Ru as the cathode and OMS MoO₃-RuO₂ as anode for overall water splitting (Figure 4F). The polarization curves (Figure 4G) show that the OMS Mo₂C/NC-Ru || OMS MoO₃-RuO₂ pair required the cell voltages of 1.62 V to drive a current density of 10 mA cm⁻², which is superior to that of commercial Pt/C || RuO₂ (1.66 V). Besides, Mo₂C/NC-Ru || OMS MoO₃-RuO₂ possessed smaller charge transfer resistance, higher and more stable current density than Pt/C || RuO₂ under the same voltage (Figure S32), suggesting the excellent water splitting performance.

3 | CONCLUSION

In summary, we have developed a facile method to construct a hierarchically multiheterogeneous ordered macroporous Mo₂C/NC-Ru for robust hydrogen production. The formed Mo₂C-NC and Ru-NC heterointerfaces exhibit a synergistic effect, boosting the Volmer and the Tafel steps in the overall alkaline HER, respectively. Furthermore, the hierarchically ordered macroporous structure endowed the catalyst with enhanced mass transport and a favorable gas release process. As a result, the well-designed OMS Mo₂C/NC-Ru showed superior HER activity in 1.0 M KOH with an extremely low overpotential of 15.5 mV at 10 mA cm⁻², an ultrasmall Tafel slope of 22.7 mV dec⁻¹, and excellent electrocatalytic durability, outperforming the commercial Pt/C. After assembling with OMS Mo₂C/NC-Ru-derived OMS MoO₃-RuO₂ to form a practical water-splitting cell, the performance also surpassed that of the state-of-the-art Pt/C || RuO₂ electrolyzer. This study provides instructive guidance for designing 3D-ordered macroporous multi-component catalysts for efficient catalytic application.

ACKNOWLEDGMENTS

This study was financially supported by the Science and Technology Development Fund, Macau SAR (File no. 0191/2017/A3, 0041/2019/A1, 0046/2019/AFJ, and 0021/2019/AIR), the University of Macau (File no. MYRG2018-00192-IAPME, and MYRG2020-00187-IAPME), and the UEA funding.

CONFLICTS OF INTEREST

The authors declare no conflicts of interest.

ORCID

Chenyang Zha  <https://orcid.org/0000-0002-7491-9146>
 Zongping Shao  <https://orcid.org/0000-0002-4538-4218>
 Kwun Nam Hui  <https://orcid.org/0000-0002-3008-8571>

REFERENCES

- Chu S, Majumdar A. Opportunities and challenges for a sustainable energy future. *Nature*. 2012;488(7411):294-303.
- Sun Y, Xue Z, Liu Q, et al. Modulating electronic structure of metal-organic frameworks by introducing atomically dispersed Ru for efficient hydrogen evolution. *Nat Commun*. 2021;12:1369.
- Podjaski F, Weber D, Zhang S, et al. Rational strain engineering in delafossite oxides for highly efficient hydrogen evolution catalysis in acidic media. *Nat Catal*. 2020; 3(1):55-63.
- Yu J, Guo Y, She S, et al. Bigger is surprisingly better: agglomerates of larger RuP nanoparticles outperform benchmark Pt nanocatalysts for the hydrogen evolution reaction. *Adv Mater*. 2018;30(39):1800047.
- Zhu J, Guo Y, Liu F, et al. Regulative electronic states around ruthenium/ruthenium disulfide heterointerfaces for efficient water splitting in acidic media. *Angew Chem Int Ed*. 2021;60(22):12328-12334.
- Jiao Y, Zheng Y, Jaroniec M, Qiao SZ. Design of electrocatalysts for oxygen-and hydrogen-involving energy conversion reactions. *Chem Soc Rev*. 2015;44(8):2060-2086.
- Roger I, Shipman MA, Symes MD. Earth-abundant catalysts for electrochemical and photoelectrochemical water splitting. *Nat Rev Chem*. 2017;1(1):1-13.
- Sun H, Xu X, Song Y, Zhou W, Shao Z. Designing high-valence metal sites for electrochemical water splitting. *Adv Funct Mater*. 2021;31(16):2009779.
- Zeng K, Zhang D. Recent progress in alkaline water electrolysis for hydrogen production and applications. *Prog Energy Combust Sci*. 2010;36(3):307-326.
- Nong S, Dong W, Yin J, et al. Well-dispersed ruthenium in mesoporous crystal TiO₂ as an advanced electrocatalyst for hydrogen evolution reaction. *J Am Chem Soc*. 2018;140(17): 5719-5727.
- Wang K, Guo Y, Chen Z, et al. Regulating electronic structure of two-dimensional porous Ni/Ni₃N nanosheets architecture by Co atomic incorporation boosts alkaline water splitting. *InfoMat*. 2022;4(6):e12251.
- Wu X, Wang Z, Zhang D, et al. Solvent-free microwave synthesis of ultra-small Ru-Mo₂C@CNT with strong metal-support interaction for industrial hydrogen evolution. *Nat Commun*. 2021;12:4018.
- Qiao Y, Yuan P, Pao CW, et al. Boron-rich environment boosting ruthenium boride on B, N-doped carbon outperforms platinum for hydrogen evolution reaction in a universal pH range. *Nano Energy*. 2020;75:104881.
- Zhang H, Zhou W, Lu XF, Chen T, Lou XW. Implanting isolated Ru atoms into edge-rich carbon matrix for efficient electrocatalytic hydrogen evolution. *Adv Energy Mater*. 2020; 10(23):2000882.
- Wang Q, Ming M, Niu S, Zhang Y, Fan G, Hu JS. Scalable solid-state synthesis of highly dispersed uncapped metal (Rh, Ru, Ir) nanoparticles for efficient hydrogen evolution. *Adv Energy Mater*. 2018;8(31):1801698.
- Kweon DH, Okyay MS, Kim SJ, et al. Ruthenium anchored on carbon nanotube electrocatalyst for hydrogen production with enhanced Faradaic efficiency. *Nat Commun*. 2020;11:1278.
- Ye S, Luo F, Xu T, et al. Boosting the alkaline hydrogen evolution of Ru nanoclusters anchored on B/N-doped graphene by accelerating water dissociation. *Nano Energy*. 2020; 68:104301.
- Li Y, Luo Y, Zhang Z, et al. Implanting Ru nanoclusters into N-doped graphene for efficient alkaline hydrogen evolution. *Carbon*. 2021;183:362-367.
- Xie Q, Wang Z, Lin L, et al. Nanoscaled and atomic ruthenium electrocatalysts confined inside super-hydrophilic carbon nanofibers for efficient hydrogen evolution reaction. *Small*. 2021; 17(38):2102160.
- Liu Y, Li X, Zhang Q, et al. A general route to prepare low-ruthenium-content bimetallic electrocatalysts for pH-universal hydrogen evolution reaction by using carbon quantum dots. *Angew Chem Int Ed*. 2020;59(4):1718-1726.
- Li W, Zhao Y, Liu Y, et al. Exploiting Ru-induced lattice strain in CoRu nanoalloys for robust bifunctional hydrogen production. *Angew Chem Int Ed*. 2021;60(6):3290-3298.
- Mahmood J, Li F, Jung SM, et al. An efficient and pH-universal ruthenium-based catalyst for the hydrogen evolution reaction. *Nat Nanotechnol*. 2017;12(5):441-446.
- Lao M, Zhao G, Li P, et al. Manipulating the coordination chemistry of Ru-N(O)-C moieties for fast alkaline hydrogen evolution kinetics. *Adv Funct Mater*. 2021;31(33):2100698.
- Wang J, Wei Z, Mao S, Li H, Wang Y. Highly uniform Ru nanoparticles over N-doped carbon: pH and temperature-universal hydrogen release from water reduction. *Energy Environ Sci*. 2018;11(4):800-806.
- Wu YL, Li X, Wei YS, et al. Ordered macroporous superstructure of nitrogen-doped nanoporous carbon implanted with ultrafine Ru nanoclusters for efficient pH-universal hydrogen evolution reaction. *Adv Mater*. 2021;33(12):2006965.
- Zheng Y, Jiao Y, Zhu Y, et al. High electrocatalytic hydrogen evolution activity of an anomalous ruthenium catalyst. *J Am Chem Soc*. 2016;138(49):16174-16181.
- He Q, Tian D, Jiang H, et al. Achieving efficient alkaline hydrogen evolution reaction over a Ni₅P₄ catalyst incorporating single-atomic Ru sites. *Adv Mater*. 2020;32(11):1906972.
- Zhou P, Tao L, Tao S, et al. Construction of nickel-based dual heterointerfaces towards accelerated alkaline hydrogen evolution via boosting multi-step elementary reaction. *Adv Funct Mater*. 2021;31(46):2104827.
- Salah A, Ren HD, Al-Ansi N, et al. Ru/Mo₂C@NC Schottky junction-loaded hollow nanospheres as an efficient hydrogen evolution electrocatalyst. *J Mater Chem A*. 2021;9(36): 20518-20529.
- Chen J, Zhang H, Yu J, et al. Self-catalyzed formation of strongly interconnected multiphase molybdenum-based composites for efficient hydrogen evolution. *Carbon Energy*. 2022; 4(1):77-87.
- Liu H, Li X, Chen L, et al. Monolithic Ni-Mo-B bifunctional electrode for large current water splitting. *Adv Funct Mater*. 2021;32(4):2107308.

32. Xu W, Lu Z, Sun X, Jiang L, Duan X. Superwetting electrodes for gas-involving electrocatalysis. *Acc Chem Res.* 2018;51(7):1590-1598.
33. Kou T, Wang S, Shi R, et al. Periodic porous 3D electrodes mitigate gas bubble traffic during alkaline water electrolysis at high current densities. *Adv Energy Mater.* 2020;10(46):2002955.
34. Wang L, Huang X, Jiang S, et al. Increasing gas bubble escape rate for water splitting with nonwoven stainless steel fabrics. *ACS Appl Mater Interfaces.* 2017;9(46):40281-40289.
35. Zhang Q, Xiao W, Guo WH, et al. Macroporous array induced multiscale modulation at the surface/interface of Co(OH)₂/NiMo self-supporting electrode for effective overall water splitting. *Adv Funct Mater.* 2021;31(33):2102117.
36. Li W, Liu J, Guo P, et al. Co/CoP heterojunction on hierarchically ordered porous carbon as a highly efficient electrocatalyst for hydrogen and oxygen evolution. *Adv Energy Mater.* 2021;11(42):2102134.
37. Jia J, Xiong T, Zhao L, et al. Ultrathin N-doped Mo₂C nanosheets with exposed active sites as efficient electrocatalyst for hydrogen evolution reactions. *ACS Nano.* 2017;11(12):12509-12518.
38. Wang K, Hui KN, Hui KS, Peng S, Xu Y. Recent progress in metal-organic framework/graphene-derived materials for energy storage and conversion: design, preparation, and application. *Chem Sci.* 2021;12(16):5737-5766.
39. Yao W, Chen J, Wang Y, et al. Nitrogen-doped carbon composites with ordered macropores and hollow walls. *Angew Chem Int Ed.* 2021;60(44):23729-23734.
40. Béjar J, Álvarez-Contreras L, Ledesma-García J, Arjona N, Arriaga LG. An advanced three-dimensionally ordered macroporous NiCo₂O₄ spinel as a bifunctional electrocatalyst for rechargeable Zn-air batteries. *J Mater Chem A.* 2020;8(17):8554-8565.
41. Lu B, Guo L, Wu F, et al. Ruthenium atomically dispersed in carbon outperforms platinum toward hydrogen evolution in alkaline media. *Nat Commun.* 2019;10:631.
42. Wang D, Liu T, Wang J, Wu Z. N, P (S) Co-doped Mo₂C/C hybrid electrocatalysts for improved hydrogen generation. *Carbon.* 2018;139:845-852.
43. Cui W, Cheng N, Liu Q, Ge C, Asiri AM, Sun X. Mo₂C nanoparticles decorated graphitic carbon sheets: biopolymer-derived solid-state synthesis and application as an efficient electrocatalyst for hydrogen generation. *ACS Catal.* 2014;4(8):2658-2661.
44. Cabán-Acevedo M, Stone ML, Schmidt JR, et al. Efficient hydrogen evolution catalysis using ternary pyrite-type cobalt phosphosulphide. *Nat Mater.* 2015;14(12):1245-1251.
45. Baek DS, Jung GY, Seo B, et al. Ordered mesoporous metastable α -MoC_{1-x} with enhanced water dissociation capability for boosting alkaline hydrogen evolution activity. *Adv Funct Mater.* 2019;29(28):1901217.
46. Lee SH, Kim J, Chung DY, et al. Design principle of Fe-N-C electrocatalysts: how to optimize multimodal porous structures? *J Am Chem Soc.* 2019;141(5):2035-2045.
47. Zhang X, Han X, Jiang Z, et al. Atomically dispersed hierarchically ordered porous Fe-N-C electrocatalyst for high-performance electrocatalytic oxygen reduction in Zn-Air battery. *Nano Energy.* 2020;71:104547.
48. Qiao M, Wang Y, Wang Q, et al. Hierarchically ordered porous carbon with atomically dispersed FeN₄ for ultraefficient oxygen reduction reaction in proton exchange membrane fuel cells. *Angew Chem Int Ed.* 2020;59(7):2688-2694.
49. Liu M, Wang JA, Klysubun W, et al. Interfacial electronic structure engineering on molybdenum sulfide for robust dual-pH hydrogen evolution. *Nat Commun.* 2021;12:5260.
50. Ji L, Wang J, Teng X, Meyer TJ, Chen Z. CoP Nanoframes as bifunctional electrocatalysts for efficient overall water splitting. *ACS Catal.* 2020;10(1):412-419.
51. Liu Y, Liu S, Wang Y, et al. Ru modulation effects in the synthesis of unique rod-like Ni@Ni₂P-Ru heterostructures and their remarkable electrocatalytic hydrogen evolution performance. *J Am Chem Soc.* 2018;140(8):2731-2734.

SUPPORTING INFORMATION

Additional supporting information may be found in the online version of the article at the publisher's website.

How to cite this article: Wang K, Wang S, Hui KS, et al. Synergistically boosting the elementary reactions over multiheterogeneous ordered macroporous Mo₂C/NC-Ru for highly efficient alkaline hydrogen evolution. *Carbon Energy.* 2022; 4:856-866. doi:10.1002/cey2.188